




Article

Depletion of Fumarate Hydratase, an Essential TCA Cycle Enzyme, Drives Proliferation in a Two-Step Model

Balakrishnan Solaimuthu ¹, Michal Lichtenstein ¹, Arata Hayashi ¹, Anees Khatib ¹, Inbar Plaschkes ², Yuval Nevo ², Mayur Tanna ¹, Ophry Pines ^{3,*} and Yoav D. Shaul ^{1,*}

¹ Department of Biochemistry and Molecular Biology, The Institute for Medical Research Israel-Canada, Faculty of Medicine, Hebrew University of Jerusalem, Jerusalem 9112001, Israel

² Info-CORE, Bioinformatics Unit of the I-CORE Computation Center, Hebrew University of Jerusalem, Jerusalem 9112001, Israel

³ Department of Microbiology and Molecular Genetics, The Institute for Medical Research Israel-Canada, Faculty of Medicine, Hebrew University of Jerusalem, Jerusalem 9112001, Israel

* Correspondence: ophryp@ekmd.huji.ac.il (O.P.); yoav.shaul@mail.huji.ac.il (Y.D.S.)

Simple Summary: Fumarate hydratase (FH) is an evolutionary conserved TCA cycle enzyme and has a moonlight function in the DNA damage response (DDR). FH has a contradictory function, as it is pro-survival through its role in the TCA cycle, yet its loss can drive tumorigenesis. Here, we solve this contradiction and show that in both non-cancerous (HEK-293T) and cancerous cell lines (HepG2), the cell response to FH loss is separated into two distinct time frames. During the early stages of FH loss, cell proliferation and DNA damage repair are inhibited. However, over time, cells overcome the FH loss and form proliferative knockout stable clones. Furthermore, we discovered that the impaired DDR induces mutations enriched in central signaling pathways, such as JAK/STAT3, allowing the cells to circumvent FH and TCA cycle loss.



Citation: Solaimuthu, B.;

Lichtenstein, M.; Hayashi, A.; Khatib, A.; Plaschkes, I.; Nevo, Y.; Tanna, M.; Pines, O.; Shaul, Y.D. Depletion of Fumarate Hydratase, an Essential TCA Cycle Enzyme, Drives Proliferation in a Two-Step Model. *Cancers* **2022**, *14*, 5508. <https://doi.org/10.3390/cancers14225508>

Academic Editor: Kim Rosalie Kampen

Received: 29 September 2022

Accepted: 4 November 2022

Published: 9 November 2022

Publisher's Note: MDPI stays neutral with regard to jurisdictional claims in published maps and institutional affiliations.

Abstract: Fumarate hydratase (FH) is an evolutionary conserved TCA cycle enzyme that reversibly catalyzes the hydration of fumarate to L-malate and has a moonlight function in the DNA damage response (DDR). Interestingly, FH has a contradictory cellular function, as it is pro-survival through its role in the TCA cycle, yet its loss can drive tumorigenesis. Here, we found that in both non-cancerous (HEK-293T) and cancerous cell lines (HepG2), the cell response to FH loss is separated into two distinct time frames based on cell proliferation and DNA damage repair. During the early stages of FH loss, cell proliferation rate and DNA damage repair are inhibited. However, over time the cells overcome the FH loss and form knockout clones, indistinguishable from WT cells with respect to their proliferation rate. Due to the FH loss effect on DNA damage repair, we assumed that the recovered cells bear adaptive mutations. Therefore, we applied whole-exome sequencing to identify such mutated genes systematically. Indeed, we identified recurring mutations in genes belonging to central oncogenic signaling pathways, such as JAK/STAT3, which we validated in impaired FH-KO clones. Intriguingly, we demonstrate that these adaptive mutations are responsible for FH-KO cell proliferation under TCA cycle malfunction.

Keywords: cancer metabolism; DNA damage; fumarate hydratase; TCA cycle



Copyright: © 2022 by the authors. Licensee MDPI, Basel, Switzerland. This article is an open access article distributed under the terms and conditions of the Creative Commons Attribution (CC BY) license (<https://creativecommons.org/licenses/by/4.0/>).

1. Introduction

Fumarate hydratase (FH) is a TCA cycle enzyme that catalyzes the hydration of fumarate to L-malate (1). Despite its essential role in central carbon metabolism, FH is inactive or absent in several tumors, such as hereditary leiomyomatosis and renal cell cancer (HLRCC) (2). This lack of functional FH results in the significant rewiring of the cellular metabolism as the cells accumulate fumarate and demonstrate a fermentative metabolism, which includes reduced oxygen consumption and elevated lactate secretion (3). Accumulated fumarate in cells functions as an “oncometabolite” (4), which inhibits

α -ketoglutarate (α KG)-dependent dioxygenases and histone DNA demethylases (5) and stabilizes the hypoxia-induced factor 1 alpha (HIF1 α) (6). Moreover, accumulated fumarate induces the epithelial-mesenchymal transition (EMT) program (7) that is associated with high-grade tumors (8) by altering the epigenetic landscape of these cells. Together, FH has contradictory cellular functions, as it is pro-survival through its role in the TCA cycle and functions as a tumor suppressor in tumorigenesis. However, a comprehensive cellular mechanism to explain these opposing roles of FH is still missing.

In addition to its localization in the mitochondria, FH is also present in the cytosol/nucleus, where it participates in the DNA damage response (DDR) (9). In the nucleus, FH converts malate to fumarate, which, upon the induction of DNA breaks, inhibits the KDM2B-mediated H3K36me2 demethylation, resulting in non-homologous end-joining repair (10). However, the function of fumarate in the DDR is still unclear, as it also suppresses the DDR by inhibiting KDM4B (11). Here, we show that the effect of FH loss in cells is divided into two time frames. In the early stages of FH loss, the cells are under stress, do not proliferate, and inhibit DDR. Consequently, this loss causes the accumulation of mutations in the FH-KO cells, enriched within genes encoding components of central oncogenic pathways. These adaptive mutations provide the long-term FH-KO cells with the capability to proliferate even in the absence of a functional TCA.

2. Materials and Methods

2.1. Cell Lines and Cell Culture

The cell lines HEK-293T and HepG2 were procured from the American Type Culture Collection (ATCC) and were cultured in DMEM supplemented with 10% FBS (Biological industries, Kibbutz Beit-Haemek, Israel). All cells were cultured at 37 °C with 5% CO₂.

2.2. Cell Lysis and Immunoblotting

Cells were rinsed twice with ice-cold PBS and lysed with RIPA lysis buffer (20 mM Tris pH 7.4, 137 mM NaCl, 10% glycerol, 1% Triton X-100, 0.5% deoxycholate, 0.1% SDS, 2.0 mM ethylenediaminetetraacetic acid (EDTA, pH 8.0), complete EDTA free Protease inhibitor cocktail tablets (1 tablet per 50 mL RIPA) (Sigma-Aldrich Israel, Rehovot, Israel, #11836170001) and phosphatase inhibitor cocktail (100 \times) (Bimake, Houston, TX, USA, # B15001-A and B). The lysates were cleared by centrifugation at 13,000 rpm at 4 °C in a microcentrifuge for 10 min. The protein concentration was determined by Bio-Rad Protein Assay Dye Reagent Concentrate (Bio-Rad, Hercules, CA, USA, #5000006). Proteins were denatured by adding SDS sample buffer (5 \times) and boiling for 5 min, then resolved by 10% SDS-PAGE, transferred onto a 0.45 μ m PVDF membrane (Immobilon-P Transfer membrane) (Merck Millipore, Carrigtwohill, Ireland, Co, #IPV00010), and probed with the appropriate antibodies.

2.3. Exome Sequencing Preparation and Analysis

The DNA was extracted from HEK-293T cells using DNeasy Blood & Tissue Kit (QIAGEN, Hilden, Germany, (#69504)). The samples were prepared and sequenced in Bio Basic Asia Pacific Pte Ltd (Singapore) and analyzed by our faculty bioinformatics unit. Specifically, we applied Mutect2 (from the GATK tools) for calling somatic short mutations (single nucleotide (SNA) and insertions/deletions). Mutect2 uses a Bayesian somatic genotyping model and the assembly-based machinery of GATK's HaplotypeCaller. We used the "Tumor with matched normal" mode with a joint analysis of multiple samples. Samples of FH KO clones were all defined as tumor samples, while the WT cell line was defined as normal. The resulting VCF was further filtered using the FilterMutectCalls tool with default parameters. Variants that passed the filter were annotated by the wANNOVAR online annotation tool [1], and only those found to be located within exonic regions were kept.

2.4. Antibodies

Antibodies were obtained from the following sources: FH (#4567) and Phospho-Histone H2A.X-Ser139 (20E3 (#9718), p-STAT3-Tyr705 (#9145), STAT3 (#9139), Rabbit

β -actin (#4970), mouse β -actin (#3700) from Cell Signaling Technology (Danvers, Ma), and HRP-labeled anti-mouse (Jackson ImmunoResearch Laboratories, (West Grove, Pa), 115-035-003) and anti-rabbit (111-035-144) secondary antibodies from Jackson ImmunoResearch. For immunofluorescence assays: Goat-anti mouse-Alexa fluor 647 (Abcam, (Cambridge, UK), #ab150119), Donkey-anti rabbit-Rhodamine red X (Jackson ImmunoResearch Laboratories, 711-295-152), and Donkey anti-rabbit-Alexa fluor 488 (Jackson ImmunoResearch Laboratories, 711-545-152).

2.5. Virus Production

HEK-293T cells were co-transfected with the pcw107-V5 plasmid expressing CA-STAT3 (Addgene, (Watertown, MA, USA), #64611), VSV-G envelope plasmid, and Δ vpr lentiviral plasmid using X-TremeGene 9 Transfection Reagent (MERCCK, # 6365779001). The supernatant containing the virus was collected 48 h after transfection and spun for 5 min at 400 g to eliminate cells.

2.6. Fluorescence Microscopy

The HEK-293T (60,000 cells) and HepG2 (50,000 cells) were seeded on polylysine-coated glass coverslips in 12-well tissue culture plates. After 24 h, the slides were rinsed twice with PBS and fixed with 4% paraformaldehyde in PBS for 15 min at room temperature, followed by quenching with ammonium chloride (1% in PBS). The slides were then rinsed three times with PBS, and cells were permeabilized with 0.1% Triton X-100 in PBS (PBS-T) for 10 min. Next, the cells were gently rinsed three times with PBS and incubated for 1 h in the blocking buffer (1% BSA in PBS-T), followed by primary antibodies for 2 h (FH and γ H2AX 1:200 each in 1% BSA in TBST) at room temperature. Next, the cells were rinsed three times with PBS, incubated with secondary antibodies (diluted 1:200 in 1% BSA in TBST), and Phalloidin-iFluor 555 Reagent (Abcam, ab176756) for 1 h at room temperature in the dark, and washed three times with PBS. Slides were mounted on glass coverslips using Vectashield (Vector Laboratories, Newark, CA, USA# H-1000). The cells were imaged on Nikon Spinning Disk/high content screening system (Nikon, Tokyo, Japan) using the 60 \times (NA = 0.95, dry, CFI Plan-Apochromat Lambda) and 100 \times (NA = 1.4, oil, Plan-Apochromat). This microscope is equipped with a spinning disk Yokogawa W1 Spinning Disk, 2 sCMOS ZYLA cameras, and 405 nm, 488 nm, 561 nm, and 638 nm laser. While the 20 \times (NA = 0.5, dry, WD 2.1 mm, pH1) images were acquired using the Eclipse NI-U upright microscope (Nikon), equipped with DS-QI2 MONO-cooled digital microscope camera 16 MP. The image analyses were performed using the NIS Elements software package for multi-dimensional experiments and exported as 16-bit. The pictures were slightly adjusted (levels) using Adobe Photoshop (San Jose, CA, USA).

2.7. CRISPR/Cas9-Mediated Knockout Cell Lines

For CRISPR-Cas9-mediated genome editing we used pSpCas9(BB)-2A-Puro (PX459) V2.0 (Addgene Plasmid #62988), and PX458-GFP (Addgene Plasmid #48138). Transfected cells for the long-term experiments were then subjected to single-cell isolation by limiting dilution in 96-well plates. Editing of the FH locus was confirmed by assessing protein levels by Western Blot. Primers used for cloning non-targeting control (NTC), NTC-sgRNA 5' caccgGCGCTTCCGCGGCCCGTTCAA 3' and 5' aaacTTGAACGGGCCGCGGAAGCGg; 3'; FH-gRNA1 5' caccgACATGATCGTTGGGATGCAC 3' and 5' aaacGTGCATCCCAACGATCATGTc 3'; FH-gRNA2 5' caccgGGTATCATATTCTATCCGGA 3' and 5' aaacTCCGGATA-GAATATGATAACCc 3'; FHgRNA3 5' caccgAATAATGAAGGCAGCAGATG 3' and 5' aaacCATCTGCTGCCTTATTATTc 3'; DPYD-gRNA1 5' caccgTGTGCTCAGTAAGGACTCGG 3' and 5' aaacCCGAGTCCTTACTGAGCACAc 3'.

2.8. Cell Proliferation Assay

For the IncuCyte live-cell imaging system (Sartorius, Goettingen, Germany), the cells were seeded in 96-well plates at a density of 800 cells/well (HEK-293T or HepG2, WT, FH-KO

short time, and stable clones). The cell proliferation rate was monitored every two hours at intervals using the IncuCyte live-cell imaging system. After 48 h for HEK-293T or 70 h for HepG2, the plates were removed, and the proliferation assay results were compiled from six wells from each group. Then, the data were analyzed and plotted as a graph. For Cell Titer-Glo assays, the cells were seeded in white 96-well plates (Greiner, Kremsmünster, Austria) at a density of 800 cells/well. Cell viability was assessed with Cell Titer-Glo (Promega, Madison, WI, USA #G7571) after 1, 3, and 5 days following seeding, and luminescence was measured with Cytation 3 Multi-Mode Reader (Biotek, Winooski, VT, USA).

2.9. RNA Preparation, qPCR Analysis, and RNA-seq

Total RNA was isolated from cells using the NucleoSpin[®] RNA Kit (MACHEREY-NAGEL, Duren, Germany), and reverse transcription was performed using the qScript cDNA Synthesis Kit (Quantbio, Beverly, MA, USA). The resulting cDNA was diluted in DNase-free water (1:10) before quantification by real-time quantitative PCR. The mRNA transcription levels were measured using 2× qPCRBIO SyGreen Blue Mix Hi-ROX (PCR Biosystems, London, UK) and StepOnePlus (Applied Biosystems, Waltham, MA, USA). The data are expressed as the ratio between the expression level of IL-6 mRNA and that of Actin. The primers used for the qPCR analysis were obtained from Integrated DNA Technology (Table 1):

Table 1. qPCR primers used in this study and their sequences.

Gene	Forward	Reverse
IL-6	ACTCACCTCTTCAGAACGAATTG	CCATCTTTGGAAGGTTTCAGGTTG
β-Actin	CCAACCGCGAGAAGATGA	CCAGAGGCGTACAGGGATAG
VIM	ACCCGCACAACGAGAAGGT	ATTCTGCTGCTCCAGGAAGCG
TWIST	TGCGGAAGATCATCCCCAGG	ATTCTGCTGCTCCAGGAAGCG
MMP9	TGTACCGCTATGGTTACTCTCG	GGCAGGGACAGTTGCTTCT

For RNA-seq analysis, the RNA quality was determined using a Tap station. Only RNA samples with 9–10 RIN were subjected to sequencing at our faculty Genomic Applications Laboratory of the Core Research Facility. The RNA-seq results were analyzed by our faculty bioinformatics unit.

2.9.1. Metabolite Supplementation

FH was knocked out from HEK-293T cells, and after 48 h, 1000 cells/well were seeded in white 96-well plates for an additional 24 h. Following that, the cells were treated with DMSO (control), 250 μM diethyl malate (Sigma Aldrich, #W237418), or 250 μM mono-ethyl fumarate (Sigma Aldrich, #12842225G). The metabolites were added twice a day for a total of three days. Cell viability was measured using the Cell Titer-Glo kit, and luminescence was measured with Cytation 3 Multi-Mode Reader.

2.9.2. Comet Assay

The assay was conducted according to the Abcam comet assay kit (#ab238544) protocol. Briefly, 35 μL of suspended cells (1×10^6 /mL) was mixed with 150 μL agarose, and 35 μL of this mixture was added to each agar-precoated slide. After incubation, the slides were immersed in pre-chilled lysis buffer for one hour and replaced with a pre-chilled alkaline solution (300 mM NaOH, 1 mM EDTA-Na₂, pH 13) for 30 min, all at 4 °C and in the dark. Then the slides were electrophoresed in TBE buffer for 20 min at 35 volts (1 V/cm). After the run, the slides were dried, immersed twice with pre-chilled DI-H₂O for 2 min, dehydrated in cold 70% ethanol for 5 min, stained with vista green DNA Dye (from the kit) at room temperature for 15 min, and analyzed using a fluorescence microscope

(FITC filter) (Nikon, Tokyo, Japan, Eclipse Ni). Quantification was performed using the software Comet Assay IV to determine the average comet tail lengths.

2.9.3. Statistical Analysis

Data are shown as mean \pm SD from at least three independent biological experiments. All the statistical analyses were performed using the R (version 4.2.0) or GraphPad Prism (version 8.0) statistical analysis programs. In most figures, the *p*-values measured the difference between the indicated samples and quantified using the unpaired two-tailed Student's *t*-test. Data distribution was assumed to be normal, but this was not formally tested. The significance of the mean comparison is present in each figure. The pie chart was generated using the R package ggplot2, and the *p*-value was calculated using Fischer's exact test. Chromosome with mutation location was generated using R package RIdeogram, and the gene list was taken from Piovesan *St. al.* [2]. One sample proportion test was applied to calculate the significance of the mutation number for each chromosome. Benjamini-Hochberg procedure was used to normalize the result. Information about the chromosomal mutations, including the mutation site, was extracted from HEK293T cells' exon sequence results, then plotted on the chromosome map using the R package RIdeogram. Mutations with a frequency of four or more are assumed to be a frequent mutation.

3. Results

3.1. Short-Term FH Loss Inhibits Cell Proliferation

We first sought to determine the impact of FH loss on the cell proliferation rate and, in particular, to characterize the difference between short-term and long-term effects. We found that after five days of CRISPR-Cas9 induction in HEK-293T cells (non-cancerous human embryonic kidney cell line) and one day with the HepG2 (hepatocellular carcinoma cell line), FH expression levels were almost completely abolished (Figure 1a). Nevertheless, after a few days of the CRISPR-Cas9 induction, we observed that in the polyclonal population of FH-KO cells, the enzyme expression gradually returned to WT levels. These findings are consistent with the role of FH in proliferation, as cells that have escaped the knockout and still express FH have a growth advantage over those lacking the enzyme (FH-KO). This conclusion is further supported by the short-term knockout of the *DPYD*, a non-essential metabolic gene [3], which, even after seven days, retained a low expression level (Figure S1a). Remarkably, despite this impact on cell proliferation, we could generate stable FH-KO clones (FH-Clone-1 and 2) for both cell lines (Figure 1a), suggesting a long-term cellular mechanism that enables cells to overcome FH loss.

We conducted real-time monitoring of the effect of FH loss on cell growth using the Incucyte Live-Cell analysis system. We found that in both cell lines, the proliferation rate of the two different short-term FH-KO cells was significantly lower than WT cells (Figures 1b,c and S1b). Moreover, supplementing the medium with fumarate (FH substrate) had no effect (Figure S1c), while malate (FH product) supported FH-KO cell growth (Figure 1d). Therefore, the initial response of cells to FH loss is inhibition of proliferation due to TCA cycle impairment. Nevertheless, several short-term FH-KO cells can overcome this proliferation obstacle and convert into long-term growing clones. Collectively, we reveal that the impact of FH loss on cell proliferation is divided into two phases, based on the time from CRISPR-Cas9 induction: short- and long-term. Furthermore, the ability of cells to proliferate without a functional FH demonstrates that these cells have adapted to the metabolic change.

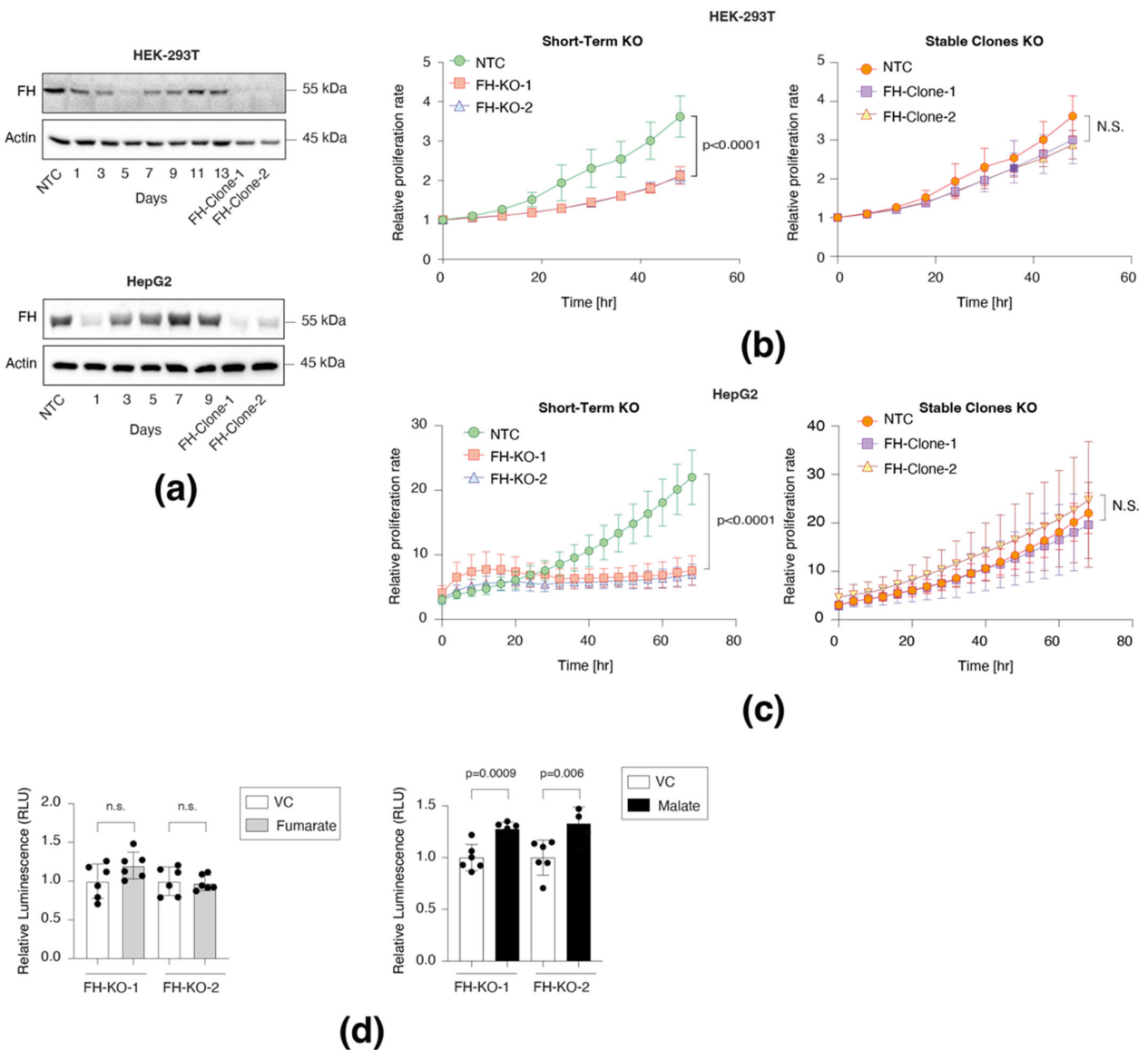


Figure 1. Short-term FH loss inhibits cell proliferation. (a) FH expression profile in short-term and long-term knockout cell lines. FH was silenced in HEK-293T and HepG2 using the CRISPR-Cas9 system and then subjected to 24 h of puromycin selection. At the indicated times post-selection (short-term), the cells were lysed and subjected to immunoblotting using the indicated antibodies. FH-Clone-1 and FH-Clone-2 are long-term FH knockout clones, and NTC is a non-targeted control. (b) FH was knocked out from HEK-293T, and then two days post puromycin selection, the cells were subjected to IncuCyte for proliferation analysis and monitored every 2 h up to 48 h (left). Additionally, two stable FH-KO clones were subjected to the same procedure for 48 h (right). NTC is non-targeted control. The analysis of both short-term and long-term was conducted simultaneously. Each bar represents the mean \pm SD for $n = 6$. The p -value was determined by Student's t -test. N.S. = no statistically significant differences between the samples. (c) HepG2 cells were analyzed similarly to HEK-293T above by IncuCyte for 70 h. Each bar represents the mean \pm SD for $n = 6$. The p -value was determined by Student's t -test. N.S. = no statistically significant differences between the samples. (d) The proliferation rate of FH short-term knockouts was not rescued by supplementing fumarate (mono-ethyl fumarate, left) and only partially rescued by malate (diethyl malate, right). FH was knocked out in HEK-293T cells and then treated with vehicle control (DMSO, VC), fumarate (250 μ M), or malate (250 μ M) for three days. The p -values were determined by Student's t -test. The uncropped Western Blot images can be found in Figure S4.

3.2. Short-Term FH Loss Induces DNA Damage

Recent studies indicated that FH cellular function is more complex than initially thought, as it is also localized in the nucleus, where it functions in the DDR [4,5]. Indeed, the immediate effect of FH KO (short-term) in both HEK-293T (Figure 2a) and HepG2 (Figure 2b) was stepwise induction in H2A.X phosphorylation (γ -H2AX), which is negatively correlated with FH loss. In contrast, this phosphorylation, a sensitive marker of DNA double-strand breaks [6], is absent in the long-term FH-KO cells, suggesting that DNA damage is impaired at the early stages of FH loss. This finding supports our notion that DNA damage functions as an integral part of the cell adaptation to FH loss.

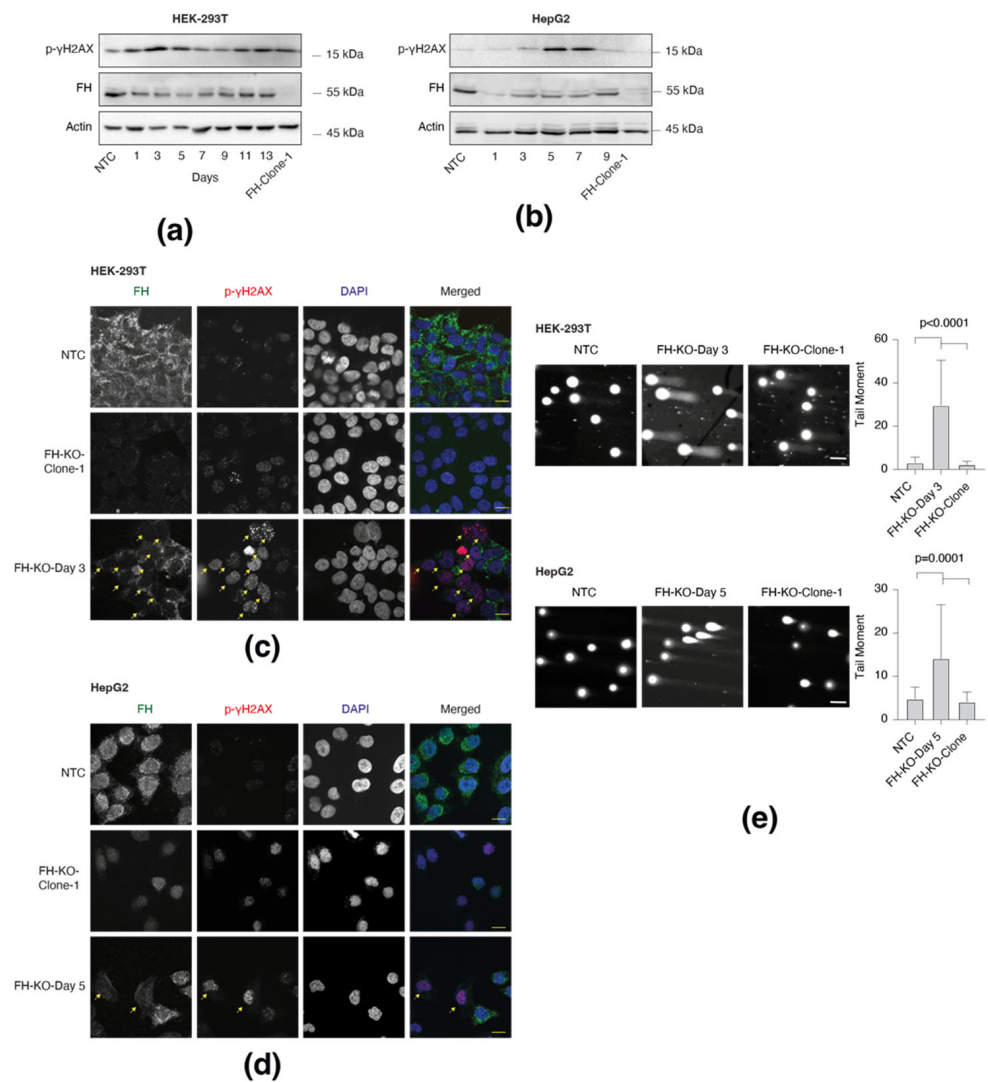


Figure 2. Short-term FH loss induces DNA damage. (a) γ H2AX phosphorylation is elevated in short-term FH loss in HEK-293T cells. FH expression was silenced in HEK-293T using the CRISPR-Cas9 system. On each indicated day (post-infection), the cells were lysed and subject to Western blot using the indicated Abs. FH-KO-1 are stable long-term FH knockout clones. (b) γ H2AX phosphorylation is elevated in short-term FH-depleted HepG2 cell line as analyzed in A. (c) HEK-293T cells were fixed and stained for FH (green), p- γ H2AX (red), and DAPI (blue). Bar = 10 μ m. Arrows indicate FH knockout cells. (d) HepG2 cells analyzed as in C. Bar = 10 μ m. (e) Short-term FH loss induces DNA breaks. NTC, short-term, and long-term FH-KO cells in both HEK-293T and HepG2 were subjected to the comet assay. Representative images of each sample (left). Bar = 10 μ m. Quantification of data is reported as the number of tail moments (right); each bar represents the mean \pm SD for $n \geq 30$. The p -value was determined by Student's t -test. The uncropped Western Blot images can be found in Figure S5.

Co-staining of HEK-293T and HepG2 cells with FH and γ -H2A.X antibodies indicates that the DNA damage is specific for the short-term KO cells (Figure 2c,d). Fascinatingly, in this polyclonal population (short-term), only cells that appear as FH-KO (not stained with FH antibodies) exhibit γ -H2A.X foci. In line with these results, we show by comet assay that the short-term FH-KO cells demonstrate a significantly high level of DNA breaks versus WT and long-term clones (Figure 2e). Since the long-term FH-KO cells do not display DNA damage, despite the absence of functional FH, it suggests that the growth of these cells is a product of an adaption process. Hence, identifying the mutations induced by the FH-KO-dependent DNA damage impairment will help understand the adaption process.

3.3. Whole Exome Sequencing Analysis of Long-Term FH KO Clones

To assess the consequence of the impaired DNA damage response, we subjected 11 HEK-293T FH-KO clones and one WT (as a reference) to whole-exome sequencing (Table S1). The mutations identified in the different clones were compared to WT cells using Mutect2, a somatic variant caller [7] (Figure 3a, illustration). This analysis resulted in 14,959 FH-KO-specific variants. Next, we filtered out the variants localized in intronic regions using the wANNOVAR online annotation tool [1]. To avoid the possibility of non-specific variants, we first retained only those with more than ten reads. Then, to increase the probability of true hits, we focused only on the variants that exhibited a high percentage of reads from the total. To this end, for every variant in each FH-KO clone, we calculated the percentage of alteration out of the total reads of this sequence. This analysis allowed us to identify those with at least 30% variation reads, about 12% of the total variants (Figure S2b).

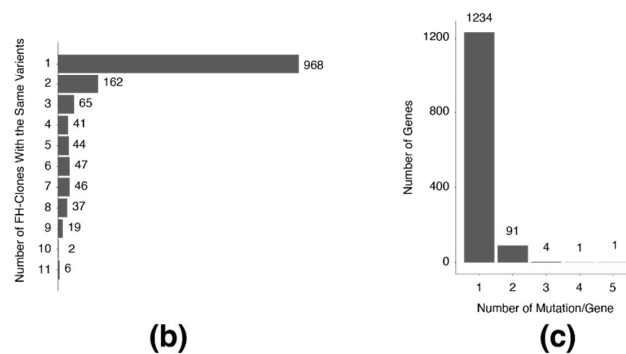
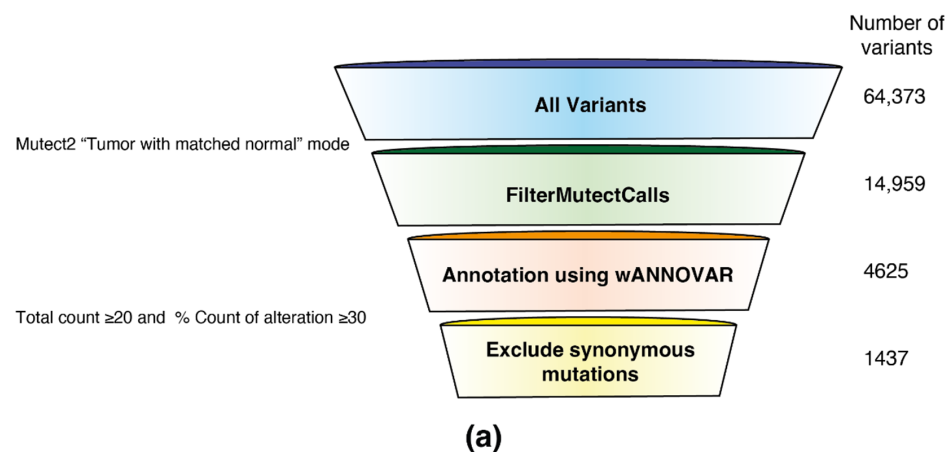


Figure 3. Exome sequencing analysis of FH knockout cells. (a) Whole-genome exome sequencing analysis and variant filtering. Variant filtering funnel scheme with the number of variants left after each filtering (right). (b) A column bar graph representing the number of FH-clones with the same variants. The number on the right of the bar indicates the number of variants. (c) A column bar graph representing the number of mutations in each gene. The number on the top of the bar indicates the number of genes.

Next, we removed all synonymous mutations, resulting in 1437 variants. We found that the majority of the genes in the list had one mutation per clone (968 variants) (Figure 3b). However, several genes had recurrent mutations in multiple clones, including six mutated in all samples (MTRF1L, IGFALS, CTSD, BMP1, PCDHB13, and FAM196A). Moreover, 97 genes were mutated in two or more locations (Figure 3c). Interestingly, we observed that the mutated genes did not distribute randomly over the chromosomes, as several are significantly more abundant on chromosomes 9, 11, and 19 (Figure S2c). These results portray a novel perception of how FH loss induces genomic mutations, which presumably provide the cells with the ability to overcome the FH-related proliferation impairment.

3.4. Long-Term FH Knockout Clones Harbor Mutations in Central Metabolic and Signaling Pathways

We inquired whether mutations detected in the previous section are associated with common biological processes. Using the Kyoto encyclopedia of genes and genomes (KEGG) pathway database (<https://www.genome.jp/kegg/pathway.html> (accessed on 1 September 2021)) [8], we discovered that these FH loss-associated mutations are present in genes of multiple metabolic pathways, such as central carbon metabolism, nucleotide biosynthesis, and amino acid metabolism (Figure 4a). Moreover, we identified that FH loss significantly induces mutations in signaling pathways (Figure S3a,b), indicating that they provide a growth advantage. Specifically, these pathways include central pro-survival signaling cascades such as the MAPK, chemokine, Wnt, and JAK/STAT3 signaling (Figure 4b). By applying the KEGG mapper color tool, we present the mutated genes in MAPK-signaling, chemokines, and JAK/STAT3 pathways (Figure S3c). These findings highlight the enrichment of FH-loss-induced mutations in central signaling pathways, indicating that these genomic impairments are not random.

3.5. FH Loss Results in STAT3 Signaling Impairment

To further examine the effect of FH loss on signaling pathways, we chose the well-known JAK/STAT3, which may provide a step in the adaption process. We demonstrated that this signaling pathway regulates HEK-293T growth since expressing a constitutively activated STAT3 (A662C, N664C, V667L, CA-STAT3) [9,10] significantly inhibited its proliferation rate (Figure 5a). Accordingly, FH-long-term loss inhibited STAT3 activity, as reflected by a reduction in tyrosine 705 phosphorylation (Y705) (Figure 5b) and repression of its downstream target, IL-6 (Figure 5c). Moreover, this change in pSTAT3 levels is reduced shortly after FH loss in both HEK-293T and HepG2 (Figure 5d). Finally, RNA seq analysis (Table S2) of the WT and FH-KO clone, followed by Gene Set Enrichment Analyses (GSEA) [11], demonstrated that FH loss significantly reduces the “Hallmark of IL6-JAK-STAT3 signaling”. Additionally, we noticed other STAT3-related hallmarks, such as “Hallmark of the epithelial-mesenchymal transition” and “Hallmark of KRAS signaling-up,” were reduced (Figure 5e). This analysis was further validated by qPCR, where the known STAT3 targets, vimentin (VIM), TWIST, MMP9, and IL-6 [12], are significantly downregulated in FH-clones 1 and 2 (Figure 5f). Interestingly, analysis of patient data using the Cbiopotal web-based (<https://www.cbioportal.org> (accessed on 1 May 2022)) tool identified two tumor samples; MPCPROJECT_0130 (Prostate Adenocarcinoma) and SD5038 (Cutaneous Melanoma), in which both IL-6 and FH are deleted. Collectively, we demonstrated that in FH-KO cells, the STAT3 signaling is impaired, which restored proliferation.

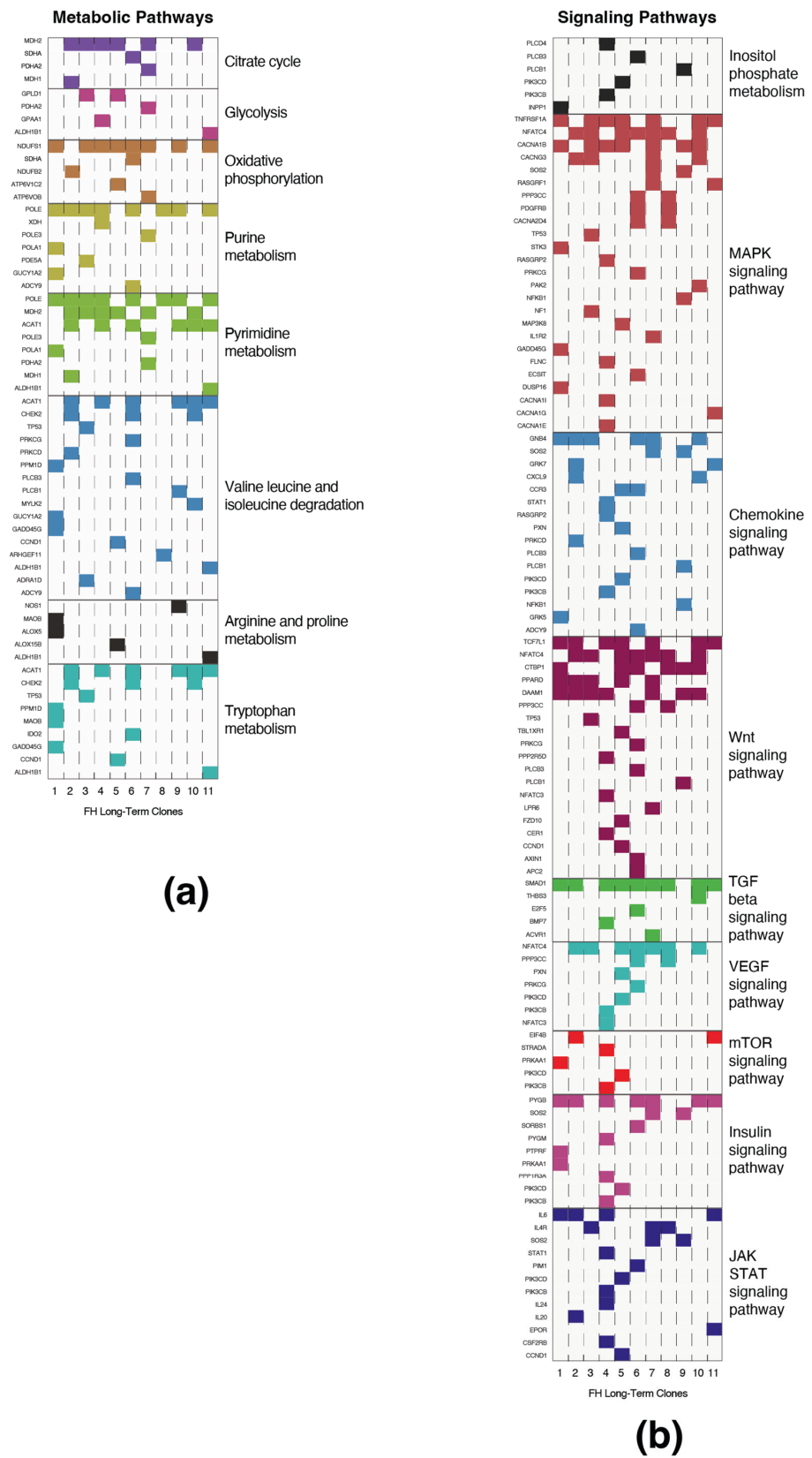


Figure 4. Long-term FH loss is accompanied by mutations in selected signaling and metabolic genes. (a) The mutated genes are presented as metabolic pathways. Each column represents a different FH-KO clone, and each row represents a different gene. The different pathways are color-coded and determined by the KEGG database. (b) The names of selected signaling pathways are color labeled as in A.

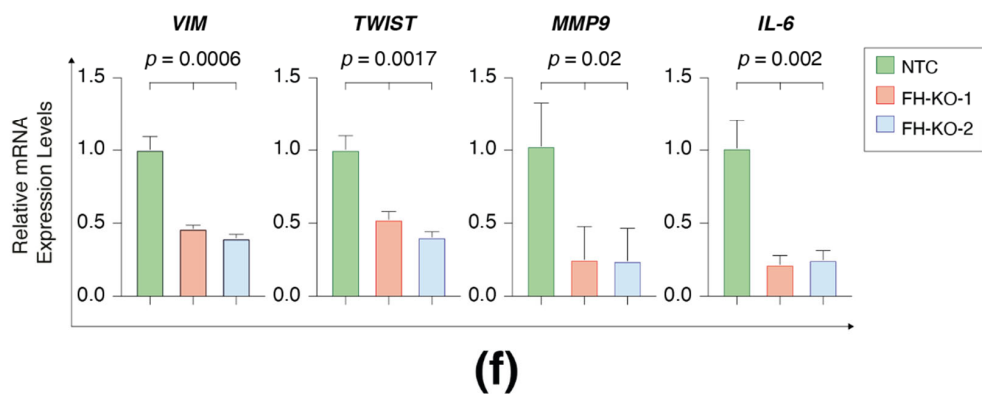
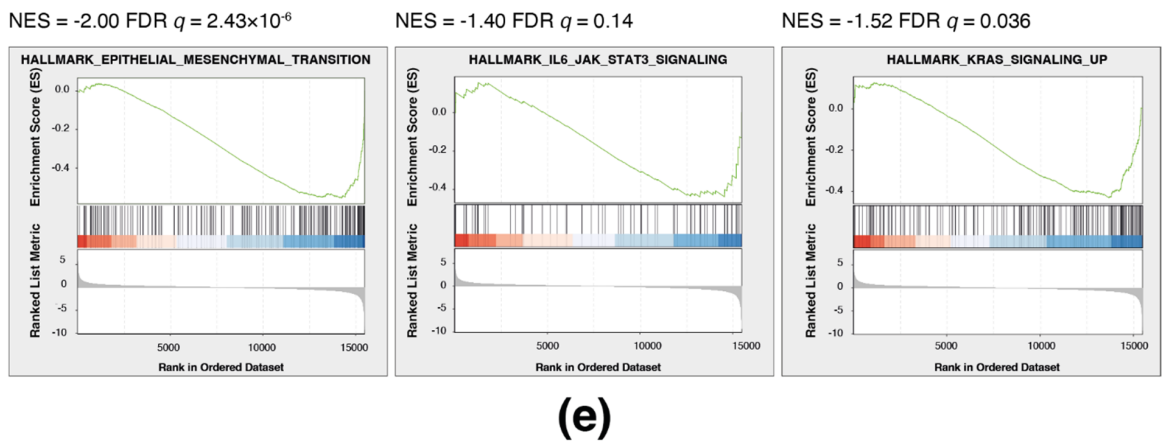
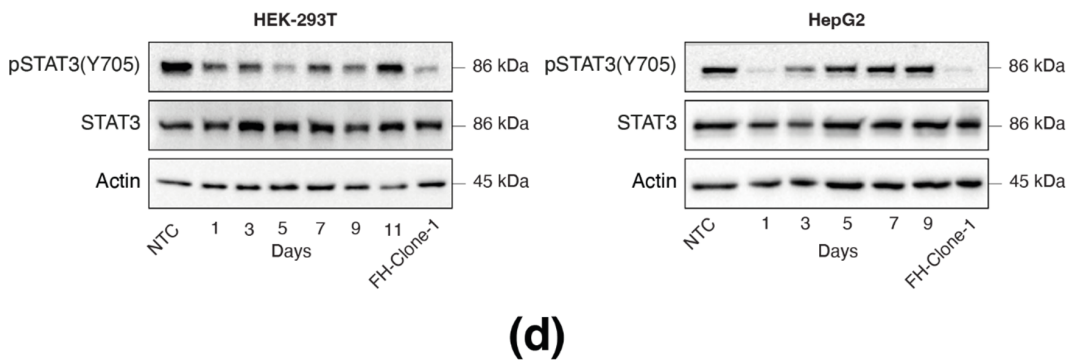
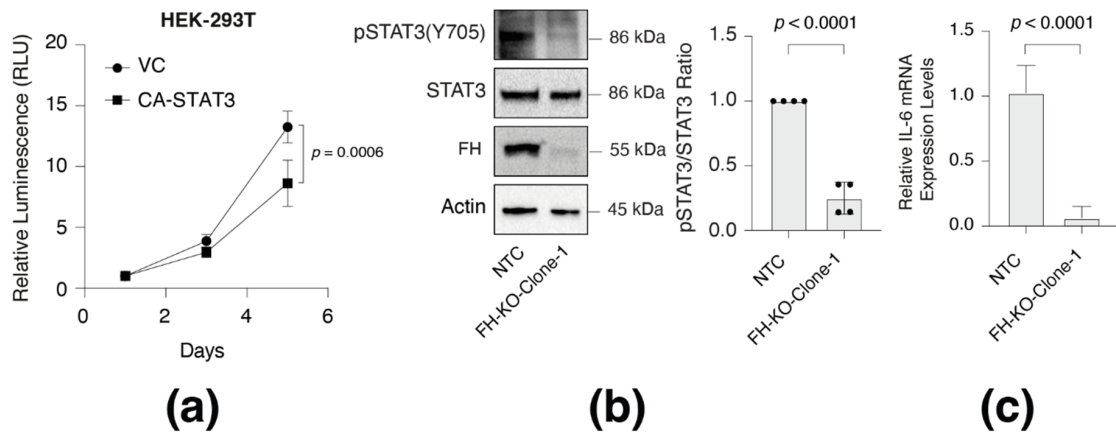


Figure 5. FH loss inhibits STAT3 signaling. (a) Constitutively activated STAT3 (CA-STAT3) inhibits cell proliferation in HEK-293T. The proliferation rates of WT and CA-STAT3 cells were measured using

CellTiter Glo. Each value represents the mean \pm SD for $n = 6$. The p -value was determined by Student's t -test. VC = vector control. (b) STAT3 phosphorylation is reduced in FH-KO-clone-1. Immunoblots representing WT HEK-293T expressing NTC and long-term FH-KO clone-1. Cells were lysed and subjected to immunoblotting using the indicated antibodies (Left). Quantification of phospho-STAT3 immunoblots normalized to total STAT3 levels; each bar represents the mean \pm SD for $n = 3$. The p -value was determined by Student's t -test (Right). NTC = non-targeted control. (c) FH loss reduces IL-6 mRNA expression level. Each bar represents the mean \pm SD for $n = 12$. The p -value was determined by Student's t -test (Right). NTC = non-targeted control. (d) FH expression profile in short-term and long-term knockout cell lines. FH was silenced in HEK-293T and HepG2 using the CRISPR-Cas9 system and then subjected to 24 h of puromycin selection. At the indicated times post-selection (short-term), the cells were lysed and subjected to immunoblotting using the indicated antibodies. FH-Clone-1 are long-term FH knockout clones, and NTC is a non-targeted control. (e) FH loss leads to reduced gene expression of the hallmark of EMT, Hallmark IL6 JAK signaling, and Hallmark of KRAS signaling. HEK-293 WT cells and FH-KO-clone-1 were subjected to RNA-Seq analysis. The expression ratio between all genes ($\sim 22,000$) was calculated and ranked based on the relative expression between the FH WT and KO. The samples were subjected to GSEA. GSEA computed the FDR q -value. (f) FH loss reduces the expression of STAT3 target genes in HEK-293T cells. The RNA was isolated from WT, FH-clone-1, and FH-clone-12 cells, and the expression of the indicated genes was determined by qPCR. Each value represents the mean \pm SD for $n = 3$. The p -value was determined by Student's t -test. The uncropped Western Blot images can be found in Figure S6.

4. Discussion

The FH enzyme is a critical component of the TCA cycle and thus plays a vital role in cell metabolism and proliferation. However, cells are capable of proliferating without this enzyme, and moreover, mutation or deletion of FH is an apparent driver of various cancers [13]. To illuminate this apparent paradox, we show that the immediate impact of FH loss is the inhibition of cell proliferation. Yet, stable knockout clones that we generated display insignificant differences in their proliferation rate compared to the WT cells. In this study, we set out to resolve this paradox and reveal the molecular mechanism by which cells shift from FH-dependent to FH-independent proliferation.

Addressing this paradox, we describe a comprehensive model that differentiates between the short-term and long-term effects of the FH knockout. We determine that the connection between these two phases of proliferation lies in the DNA damage response, which involves the moonlighting function of FH. In WT cells, FH participates in the TCA cycle, as well as in the DNA damage response [14]. However, upon the initiation of FH loss, the halted cells also become deficient in their ability to repair their DNA and therefore are prone to the accumulation of mutations (Figure 6). We found that these are not random mutations, as they are enriched in genes encoding signaling molecules. The JAK/STAT3 pathway is an example of a signaling cascade that is impaired in these long-term FH-stable clones.

Over the past twenty years, several mechanisms have been proposed to address the FH role in cancer, mainly focusing on accumulated fumarate due to enzyme loss [15,16]. In renal tumors, accumulated fumarate functions as an oncometabolite [17], which stimulates cancer-associated processes. For example, accumulated fumarate inhibits PH (prolyl-hydroxylase) activity and thus stabilizes HIF1 α at normal oxygen tensions [18,19]. Additionally, under acidic conditions, fumarate interacts with cysteine thiol groups, forming a post-translation modification termed "succination", which regulates the activity of pro-oncogenic signaling factors such as KEAP1 (Kelch Like ECH Associated Protein 1) [13]. We found that fumarate intracellular levels did not change significantly at the early stage of FH loss, and the addition of mono-ethyl fumarate esters does not alleviate short-term FH KO effects. This indicates that the proliferation inhibition is not due to vast intracellular oncometabolite accumulation. Previously, we demonstrated that FH is also found in the nucleus, where it functions in the DDR [4,5]. Specifically, FH is localized to the damage site, where it produces fumarate from malate [20,21]. However, it is becoming clear that fumarate may have both pro- and

anti-DNA damage repair roles [22,23]. We do not wish to dwell on this question regarding the fumarate function in the DDR, as long as its role in this process is established.

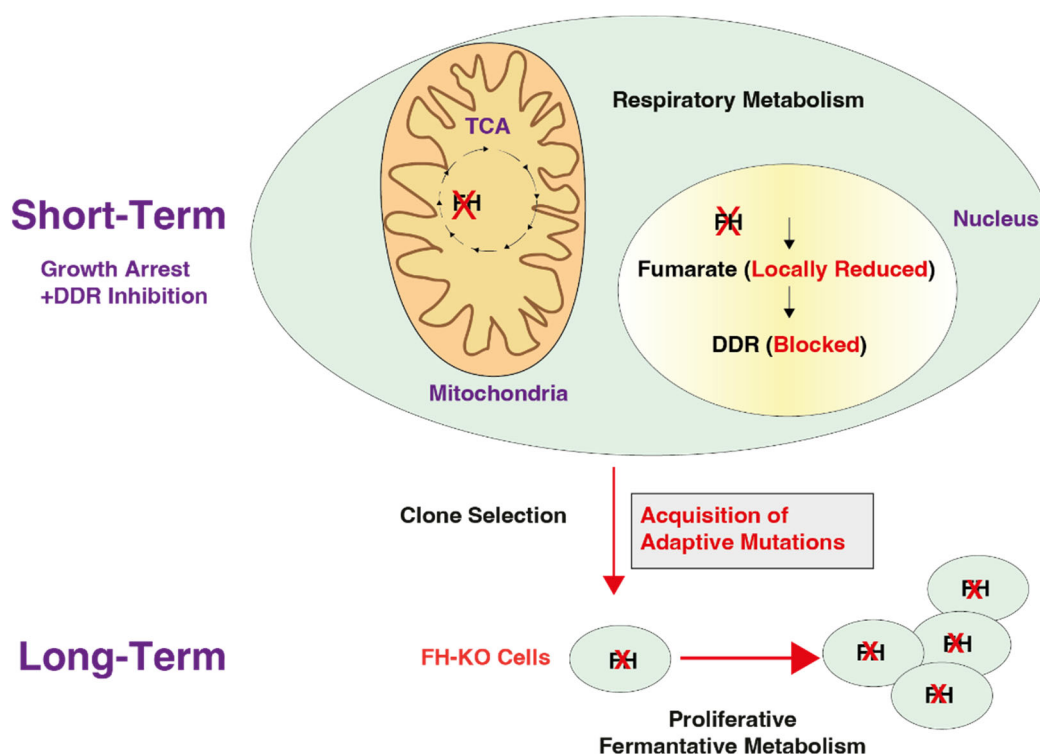


Figure 6. A scheme demonstrating the cellular behavior at the early stages of FH knockout and its long-term result in selected clones. Immediately after FH KO, the cell proliferation rate decreases as the cells lose their ability to utilize the TCA cycle and to activate the DNA damage response (DDR) (Short-Term). This blockage in the DDR induces mutagenesis that, in turn, results in the acquisition of adaptive mutations. By accumulating these mutations, the cell regains its proliferative abilities. The red cross is an indication of FH KO cells.

The execution of the EMT program induces significant changes in cell characteristics, such as their morphology and migratory capabilities [24]. Notably, the EMT program outcome is reversible, as the cells can regain their epithelial characteristics by inducing the mesenchymal-epithelial transition program (MET) [25]. Previously, Sciacovelli et al. demonstrated that FH loss in a *Fh1*^{-/-} mouse and in human FH-deficient cells (UOK262) induced the EMT program [26]. However, our study found that, in HEK-293T cells, FH loss induces the opposite MET program. Additionally, we demonstrated that FH loss affects the JAK/STAT3 signaling pathway, a central regulator of the EMT program [27]. This inconsistency in FH's role in the cell's fate could be due to the different cell line models used. Specifically, we investigated the effect of FH loss on HEK-293T, which is in an epithelial and mesenchymal hybrid state as it expresses both markers [28]. In contrast, the cells used in the other studies examined FH loss in epithelial cells. Thus, it is possible that the FH role in cell plasticity is not limited to the EMT program but has a more complex function.

5. Conclusions

The FH enzyme is a critical component of the TCA cycle and thus plays a vital role in cell metabolism and proliferation. However, cells can proliferate without this enzyme, and, moreover, mutation or deletion of FH is an apparent driver of various cancers. To illuminate this apparent paradox, we show that the immediate impact of FH loss is the inhibition of cell proliferation. Yet, we generated stable knockout clones that display insignificant differences in their proliferation rate compared to the WT cells. In this study, we set out

to resolve this paradox and reveal the molecular mechanism by which cells shift from FH-dependent to FH-independent proliferation.

Addressing this paradox, we describe a comprehensive model that differentiates between the short-term and long-term effects of the FH knockout. We determine that the connection between these two phases of proliferation lies in the DNA damage response, which involves the moonlighting function of FH. In WT cells, FH participates in the TCA cycle, as well as in the DNA damage response. However, upon initiating FH loss, the halted cells also become deficient in their ability to repair their DNA damage and therefore accumulate mutations. We learned that these are not random mutations, as they are enriched in genes encoding signaling molecules. The JAK/STAT3 pathway is an example of a signaling cascade impaired in these long-term FH stable clones.

Supplementary Materials: The following supporting information can be downloaded at: <https://www.mdpi.com/article/10.3390/cancers14225508/s1>, Figure S1: Short-term FH loss inhibits cell proliferation; Figure S2: Distribution of the different variants; Figure S3: FH loss-dependent mutations are enriched in signaling genes; Figure S4: Uncropped Western Blots of blots shown in Figure 1; Figure S5: Uncropped Western Blots of blots shown in Figure 2; Figure S6: Uncropped Western Blots of blots shown in Figure 5; Figure S7: Uncropped Western Blots of blots shown in Figures S1 and S2.

Author Contributions: Conceptualization, O.P. and Y.D.S.; Data Curation, B.S., M.L., A.H., A.K. and M.T.; Formal Analysis, A.H., I.P. and Y.N.; Funding Acquisition, O.P. and Y.D.S.; Methodology, B.S. and M.L.; Supervision, O.P. and Y.D.S.; Writing—original draft, B.S., O.P. and Y.D.S.; Writing—review and editing, B.S., O.P. and Y.D.S. All authors have read and agreed to the published version of the manuscript.

Funding: This work was supported by the Israel Science Foundation (Grant No 299/21 (Y.D.S.) and Grant 1455/17 (O.P.)) and the Israeli Cancer Association (Grant 20210079, Gedalia Doron funds (Y.D.S.)). DIP, German Israeli Project Cooperation (Grant project SCHU 25851-2, RA 1028/10-2 (O.P.)).

Institutional Review Board Statement: Not applicable.

Informed Consent Statement: Not applicable.

Data Availability Statement: The data that support the findings of this study are available from the corresponding authors upon reasonable request.

Acknowledgments: The Genomic Applications Laboratory of the Core Research Facility, The Faculty of Medicine, The Hebrew University of Jerusalem, Israel, performed the RNA-Seq data analysis.

Conflicts of Interest: The authors declare no conflict of interest.

References

1. Chang, X.; Wang, K. WANNONAR: Annotating Genetic Variants for Personal Genomes via the Web. *J. Med. Genet.* **2012**, *49*, 433. [[CrossRef](#)]
2. Piovesan, A.; Antonaros, F.; Vitale, L.; Strippoli, P.; Pelleri, M.C.; Caracausi, M. Human Protein-Coding Genes and Gene Feature Statistics in 2019. *BMC Res. Notes* **2019**, *12*, 315. [[CrossRef](#)]
3. Shaul, Y.D.; Freinkman, E.; Comb, W.C.; Cantor, J.R.; Tam, W.L.; Thiru, P.; Kim, D.; Kanarek, N.; Pacold, M.E.; Chen, W.W.; et al. Dihydropyrimidine Accumulation Is Required for the Epithelial-Mesenchymal Transition. *Cell* **2014**, *158*, 1094–1109. [[CrossRef](#)]
4. Yogev, O.; Yogev, O.; Singer, E.; Shaulian, E.; Goldberg, M.; Fox, T.D.; Pines, O. Fumarase: A Mitochondrial Metabolic Enzyme and a Cytosolic/Nuclear Component of the DNA Damage Response. *PLoS Biol.* **2010**, *8*, e1000328. [[CrossRef](#)]
5. Leshets, M.; Silas, Y.B.H.; Lehming, N.; Pines, O. Fumarase: From the TCA Cycle to DNA Damage Response and Tumor Suppression. *Front. Mol. Biosci.* **2018**, *5*, 68. [[CrossRef](#)]
6. Bonner, W.M.; Redon, C.E.; Dickey, J.S.; Nakamura, A.J.; Sedelnikova, O.A.; Solier, S.; Pommier, Y. GammaH2AX and Cancer. *Nat. Rev. Cancer* **2008**, *8*, 957–967. [[CrossRef](#)]
7. Cibulskis, K.; Lawrence, M.S.; Carter, S.L.; Sivachenko, A.; Jaffe, D.; Sougnez, C.; Gabriel, S.; Meyerson, M.; Lander, E.S.; Getz, G. Sensitive Detection of Somatic Point Mutations in Impure and Heterogeneous Cancer Samples. *Nat. Biotechnol.* **2013**, *31*, 213–219. [[CrossRef](#)]
8. Kanehisa, M.; Furumichi, M.; Sato, Y.; Kawashima, M.; Ishiguro-Watanabe, M. KEGG for Taxonomy-Based Analysis of Pathways and Genomes. *Nucleic Acids Res.* **2022**. [[CrossRef](#)]

9. Martz, C.A.; Ottina, K.A.; Singleton, K.R.; Jasper, J.S.; Wang, T.; Alley, H.M.; Cooper, Z.A.; Tetzlaff, M.; Chen, P.-L.; Flaherty, K.T.; et al. Systematic Identification of Signaling Pathways with Potential to Confer Anticancer Drug Resistance. *Sci. Signal.* **2014**, *7*, ra121. [[CrossRef](#)]
10. Rmaileh, A.A.; Solaimuthu, B.; Khatib, A.; Lavi, S.; Tanna, M.; Hayashi, A.; Yosef, M.B.; Lichtenstein, M.; Pillar, N.; Shaul, Y.D. DPYSL2 Interacts with JAK1 to Mediate Breast Cancer Cell Migration. *J. Cell Biol.* **2022**, *221*, e202106078. [[CrossRef](#)]
11. Subramanian, A.; Tamayo, P.; Mootha, V.K.; Mukherjee, S.; Ebert, B.L.; Gillette, M.A.; Paulovich, A.; Pomeroy, S.L.; Golub, T.R.; Lander, E.S.; et al. Gene Set Enrichment Analysis: A Knowledge-Based Approach for Interpreting Genome-Wide Expression Profiles. *Proc. Natl. Acad. Sci. USA* **2005**, *102*, 15545–15550. [[CrossRef](#)] [[PubMed](#)]
12. Wang, Y.; Shen, Y.; Wang, S.; Shen, Q.; Zhou, X. The Role of STAT3 in Leading the Crosstalk between Human Cancers and the Immune System. *Cancer Lett.* **2018**, *415*, 117–128. [[CrossRef](#)] [[PubMed](#)]
13. Schmidt, C.; Sciacovelli, M.; Frezza, C. Fumarate Hydratase in Cancer: A Multifaceted Tumour Suppressor. *Semin. Cell Dev. Biol.* **2020**, *98*, 15–25. [[CrossRef](#)] [[PubMed](#)]
14. Tarcic, O.; Granit, R.Z.; Pateras, I.S.; Masury, H.; Maly, B.; Zwang, Y.; Yarden, Y.; Gorgoulis, V.G.; Pikarsky, E.; Ben-Porath, I.; et al. RNF20 and Histone H2B Ubiquitylation Exert Opposing Effects in Basal-Like versus Luminal Breast Cancer. *Cell Death Differ.* **2017**, *24*, 694–704. [[CrossRef](#)]
15. Pollard, P.J.; Brière, J.J.; Alam, N.A.; Barwell, J.; Barclay, E.; Wortham, N.C.; Hunt, T.; Mitchell, M.; Olpin, S.; Moat, S.J.; et al. Accumulation of Krebs Cycle Intermediates and Over-Expression of HIF1 α in Tumours Which Result from Germline FH and SDH Mutations. *Hum. Mol. Genet.* **2005**, *14*, 2231–2239. [[CrossRef](#)] [[PubMed](#)]
16. Frezza, C.; Zheng, L.; Folger, O.; Rajagopalan, K.N.; MacKenzie, E.D.; Jerby, L.; Micaroni, M.; Chaneton, B.; Adam, J.; Hedley, A.; et al. Haem Oxygenase Is Synthetically Lethal with the Tumour Suppressor Fumarate Hydratase. *Nature* **2011**, *477*, 225–228. [[CrossRef](#)] [[PubMed](#)]
17. Sciacovelli, M.; Frezza, C. Oncometabolites: Unconventional Triggers of Oncogenic Signalling Cascades. *Free. Radic. Biol. Med.* **2016**, *100*, 175–181. [[CrossRef](#)]
18. Pollard, P.J.; Spencer-Dene, B.; Shukla, D.; Howarth, K.; Nye, E.; El-Bahrawy, M.; Deheragoda, M.; Joannou, M.; McDonald, S.; Martin, A.; et al. Targeted Inactivation of Fh1 Causes Proliferative Renal Cyst Development and Activation of the Hypoxia Pathway. *Cancer Cell* **2007**, *11*, 311–319. [[CrossRef](#)]
19. Isaacs, J.S.; Jung, Y.J.; Mole, D.R.; Lee, S.; Torres-Cabala, C.; Chung, Y.-L.; Merino, M.; Trepel, J.; Zbar, B.; Toro, J.; et al. HIF Overexpression Correlates with Biallelic Loss of Fumarate Hydratase in Renal Cancer: Novel Role of Fumarate in Regulation of HIF Stability. *Cancer Cell* **2005**, *8*, 143–153. [[CrossRef](#)]
20. Jiang, Y.; Qian, X.; Shen, J.; Wang, Y.; Li, X.; Liu, R.; Xia, Y.; Chen, Q.; Peng, G.; Lin, S.-Y.; et al. Local Generation of Fumarate Promotes DNA Repair through Inhibition of Histone H3 Demethylation. *Nat. Cell Biol.* **2015**, *17*, 1158–1168. [[CrossRef](#)]
21. Johnson, T.I.; Costa, A.S.H.; Ferguson, A.N.; Frezza, C. Fumarate Hydratase Loss Promotes Mitotic Entry in the Presence of DNA Damage after Ionising Radiation. *Cell Death Dis.* **2018**, *9*, 913. [[CrossRef](#)] [[PubMed](#)]
22. Sulkowski, P.L.; Oeck, S.; Dow, J.; Economos, N.G.; Mirfakhraie, L.; Liu, Y.; Noronha, K.; Bao, X.; Li, J.; Shuch, B.M.; et al. Oncometabolites Suppress DNA Repair by Disrupting Local Chromatin Signalling. *Nature* **2020**, *582*, 586–591. [[CrossRef](#)] [[PubMed](#)]
23. Sulkowski, P.L.; Sundaram, R.K.; Oeck, S.; Corso, C.D.; Liu, Y.; Noorbakhsh, S.; Niger, M.; Boeke, M.; Ueno, D.; Kalathil, A.N.; et al. Krebs-Cycle-Deficient Hereditary Cancer Syndromes Are Defined by Defects in Homologous-Recombination DNA Repair. *Nat. Genet.* **2018**, *50*, 1086–1092. [[CrossRef](#)]
24. Bakir, B.; Chiarella, A.M.; Pitarresi, J.R.; Rustgi, A.K. EMT, MET, Plasticity, and Tumor Metastasis. *Trends Cell Biol.* **2020**, *30*, 764–776. [[CrossRef](#)] [[PubMed](#)]
25. Brabletz, S.; Schuhwerk, H.; Brabletz, T.; Stemmler, M.P. Dynamic EMT: A Multi-tool for Tumor Progression. *EMBO J.* **2021**, *40*, e108647. [[CrossRef](#)] [[PubMed](#)]
26. Sciacovelli, M.; Gonçalves, E.; Johnson, T.I.; Zecchini, V.R.; da Costa, A.S.H.; Gaude, E.; Drubbel, A.V.; Theobald, S.J.; Abbo, S.R.; Tran, M.G.B.; et al. Fumarate Is an Epigenetic Modifier That Elicits Epithelial-to-Mesenchymal Transition. *Nature* **2016**, *537*, 544–547. [[CrossRef](#)] [[PubMed](#)]
27. Khatib, A.; Solaimuthu, B.; Yosef, M.B.; Rmaileh, A.A.; Tanna, M.; Oren, G.; Frisch, M.S.; Axelrod, J.H.; Lichtenstein, M.; Shaul, Y.D. The Glutathione Peroxidase 8 (GPX8)/IL-6/STAT3 Axis Is Essential in Maintaining an Aggressive Breast Cancer Phenotype. *Proc. Natl. Acad. Sci. USA* **2020**, *117*, 21420–21431. [[CrossRef](#)]
28. Inada, M.; Izawa, G.; Kobayashi, W.; Ozawa, M. 293 Cells Express Both Epithelial as Well as Mesenchymal Cell Adhesion Molecules. *Int. J. Mol. Med.* **2016**, *37*, 1521–1527. [[CrossRef](#)]